A Simulation of the Effects of Air-Sea Transfer Variability on the Structure of Marine Upper Layers

PATRICE KLEIN[1]

Electricité de France, 78400 Chatou, France and Institut de Mécanique Statistique de la Turbulence, 13003 Marseille, France

(Manuscript received 12 July 1979, in final form 30 July 1980)

ABSTRACT

A rather simple one-dimensional unsteady model similar to Mellor and Durbin (1975) is used to study the effects of the time variability of meteorological inputs on the evolution of the thermal stratification of marine upper layers. The physical implications of such a model are discussed, particularly with respect to the results obtained in a number of typical situations. The thermal structure of the marine upper layers in the Gulf of Lion during the COFRASOV II expedition was also simulated. Although the model is not able to reproduce all details of the marine environment, the mixed-layer deepening and sea surface temperature are predicted rather well from the known meteorological parameters. It appears in conclusion that the most important time-variability effects have been described but that the physics of the model could be improved.

1. Introduction

The marine upper layers are constantly subjected to the atmospheric effects at the air-sea interface, mainly momentum transfer, sensible and latent turbulent heat transfers, and radiative transfers. These transfers of energy constantly change the thermal and dynamic structure of the water mass, where, typically, a warm and well-mixed turbulent layer on the surface is separated from deeper and colder layers by a zone with a high-temperature gradient, the so-called thermocline. This region can also be affected by other medium- and large-scale phenomena, mainly of an advective nature. Nevertheless, vertical distributions of temperature, current and salinity in the upper marine layers generally appear to be governed by the vertical heat, momentum and salt fluxes imposed by local air-sea transfers (cf. Camp and Elsberry, 1978). This explains why most attempts at modeling of the area involve a horizontal homogeneity assumption, which leads to one-dimensional time-dependent models of the upper ocean.

Most models developed to date assume that mean temperature, salinity and horizontal velocity are quasi-uniform within a "well-mixed layer"; local values, therefore, are lumped into integrals and these models are called "integral models" (cf. Niiler and Kraus, 1977; Zilitinkevitch *et al.*, 1979). Their advantage is the rather simple computational scheme allowed. However, they require *a priori* assumptions about the integral effects of several turbulent mechanisms, of which the diversity of proposed parameterizations testifies to the lack of experimental knowledge. Another approach would be to use the available information on other turbulent flows by means of the so-called second-order turbulence closure methods. Here the assumption is that the second-order closure schemes, primarily adjusted from laboratory data, have a sufficient degree of universality to be used for modeling marine turbulence (Lumley and Khajeh-Nouri, 1974; Siess, 1975). This approach has already been successfully used for the atmospheric boundary layer (Wyngaard and Cote, 1974; Yamada and Mellor, 1975; André *et al.*, 1976; Zeman and Lumley, 1976), and a greatly simplified version was applied to the marine upper layers by Mellor and Durbin (1975). The present work takes as a point of departure this model with such improvements as the determination and inclusion of turbulent and radiative transfers at the air-sea interface, and the use of different numerical methods.

First, a discussion of the physical processes used in the model is provided. Then, a systematic study of the effect of air-sea transfer variability on the marine thermal stratification is undertaken. Indeed, air-sea transfers are essentially variable at time scales of the order of a few hours or days, due to the diurnal evolution of solar radiation and to the passage of atmospheric fronts. Because of the nonlinear nature

[1] Present affiliation: Station Zoologique 06230–Villefranche sur Mer, France.

0022-3670/80/111824-18$08.50

of the marine mechanisms, which is apparent in the equations, this temporal variation of air-sea transfers will have a quite significant effect on the response of the marine upper layers. Finally, the model is applied to the simulation, on the basis of meteorological observations, of the thermal structure evolution observed in the Gulf of Lion during the COFRASOV II expedition in July 1976. At this opportunity, the sensitivity of the model to air-sea transfer parameterization is tested and the physical consequences of air-sea transfer variability are again examined.

2. Description and discussion of the model

a. Assumptions and equations

The general hypotheses used in marine upper layer modeling concern the existence of a "spectral gap" in the energy spectrum of marine motions, the presence of an average horizontally homogeneous situation, the validity of the Boussinesq approximation, and (for the sake of simplicity) the neglect of salinity effects. They lead to the classical local equations for the first-order moments:

$$\frac{\partial \bar{Z}}{\partial t} = -\frac{\partial}{\partial z}\left(\overline{u'w'} + i\overline{v'w'} - \nu\frac{\partial \bar{Z}}{\partial z}\right) - if\bar{Z}, \quad (1)$$

$$\frac{\partial \bar{\Theta}}{\partial t} = -\frac{\partial}{\partial z}\left(\overline{\theta'w'} - \chi\frac{\partial \bar{\Theta}}{\partial z}\right) - \frac{\partial \bar{R}}{\partial z}, \quad (2)$$

where t represents time; u, v, w, are the velocity components in the orthonormal frame of reference $0, x, y, z$, where $0z$ follows the upward vertical and $0x$, $0y$ are directed to the east and north, respectively; ($\bar{Z} = \bar{U} + i\bar{V}$) is a complex notation to express the mean drift current field; $\bar{\Theta}$ is the mean temperature; $\overline{u'w'}$, $\overline{v'w'}$ and $\overline{\theta'w'}$ respectively designate the components of the Reynold's tensor (divided by density) and heat flux (divided by the product of density and specific heat); f is the Coriolis parameter; $\bar{R}$ is the radiative heat flux (°C m s^{-1}) which penetrates to the depth z; ν is the kinematic viscosity and χ the temperature molecular diffusivity.

The calculation of the vertical turbulent fluxes ($\overline{u'w'}$, $\overline{v'w'}$ and $\overline{\theta'w'}$) should require, in principle, the consideration of second-order moment equations in which third-order moments, terms involving pressure fluctuations and dissipative terms, need to be parameterized (see, e.g., Coantic, 1978). In Mellor and Yamada (1974), closure schemes are chosen for those unknowns, then simplifying assumptions are introduced which lead to the level-2 version in which tendency and diffusion terms are neglected in all second-order turbulence equations. The resulting equations after algebraic manipulation then reduce to

$$\left.\begin{aligned}\overline{u'w'} &= -l^2\left|\frac{\partial \bar{Z}}{\partial z}\right| S_M \frac{\partial \bar{U}}{\partial z}\\ \overline{v'w'} &= -l^2\left|\frac{\partial \bar{Z}}{\partial z}\right| S_M \frac{\partial \bar{V}}{\partial z}\end{aligned}\right\} \quad (3)$$

$$\overline{\theta'w'} = -l^2\left|\frac{\partial \bar{Z}}{\partial z}\right| S_H \frac{\partial \bar{\Theta}}{\partial z}, \quad (4)$$

where S_M and S_H are known stability functions of the gradient Richardson number

$$\mathrm{Ri} \equiv g\beta\frac{\partial \bar{\Theta}}{\partial z}\Big/\left|\frac{\partial \bar{Z}}{\partial z}\right|^2$$

(g is the gravity constant and β the thermal expansion coefficient of sea water); l is an integral scale defined as

$$l = \alpha\frac{\int_{-\infty}^{0} e|z|dz}{\int_{-\infty}^{0} edz}, \quad (5)$$

with α, a numerical constant; and e is the square root of turbulent kinetic energy (TKE), $e^2 \equiv \overline{u'^2} + \overline{v'^2} + \overline{w'^2}$, determined from the TKE equation which reduces here to

$$e^2 = l^2\left|\frac{\partial \bar{Z}}{\partial z}\right|^2[(S_M - \mathrm{Ri}S_H)/C_1]^{2/3}, \quad (6)$$

with C_1 a numerical constant related to dissipation rate parameterization. It should be noted that a critical value of 0.23 beyond which turbulence would die out, appears for the gradient Richardson number.

In this model, Eqs. (1) and (2) are valid locally not only in the mixed layer but also in the thermocline. The expressions of vertical turbulent fluxes (3) and (4) are given in the traditional K-theory format. The turbulent diffusivities, obtained from second-order turbulence equations, depend directly of local current shear and stability. Thus turbulent mixing is parameterized in the mixed layer and penetration of turbulence in the stable thermocline, wherein the very strong hydrostatic stability leads to turbulence suppression.

Initial conditions concern current and temperature profiles at $t = 0$. Boundary conditions are 1), heat and momentum fluxes at the air-sea interface and 2), current and temperature values at some depth $z = -D$:

$$\left.\begin{aligned}&\overline{u'w'}\big|_{z=0} = -\tau_x(t), \overline{v'w'}\big|_{z=0} = -\tau_y(t)\\ &\overline{\theta'w'}\big|_{z=0} = -H(t)\\ &\bar{U}(-D, t) = \bar{V}(-D, t) = 0\\ &\bar{\Theta}(-D, t) = \Theta_D\end{aligned}\right\}. \quad (7)$$

TABLE 1. Mechanical energy budgets. $\bar{\epsilon}$ is the dissipation rate of TKE into internal energy (IE).

Form of energy	Accumulation and transfer	Transformation	
MKE	$\frac{\partial}{\partial t}\left(\frac{\bar{U}^2+\bar{V}^2}{2}\right)+\frac{\partial}{\partial z}\left[\bar{U}\overline{u'w'}+\bar{V}\overline{v'w'}-\nu\frac{\partial}{\partial z}\left(\frac{\bar{U}^2+\bar{V}^2}{2}\right)\right]$	$=\overline{u'w'}\frac{\partial\bar{U}}{\partial z}+\overline{v'w'}\frac{\partial\bar{V}}{\partial z}-\nu\left[\left(\frac{\partial\bar{U}}{\partial z}\right)^2+\left(\frac{\partial\bar{V}}{\partial z}\right)^2\right]$	(8)
TKE	$\frac{\partial e^2}{\partial t}+\frac{\partial}{\partial z}\overline{e^2w'}\quad\frac{\partial\frac{1}{2}e^2}{\partial t}+\frac{\partial\frac{1}{2}\overline{e^2w'}}{\partial t}\quad(=0)$	$=-\left(\overline{u'w'}\frac{\partial\bar{U}}{\partial z}+\overline{v'w'}\frac{\partial\bar{V}}{\partial z}\right)+g\beta\overline{\theta'w'}-\bar{\epsilon}$	(9)
PE	$\frac{\partial}{\partial t}(-g\beta z\bar{\Theta})+\frac{\partial}{\partial z}\left(-g\beta z\overline{\theta'w'}+zg\beta\chi\frac{\partial\bar{\Theta}}{\partial z}\right)$	$=-g\beta\overline{\theta'w'}+g\beta\chi\frac{\partial\bar{\Theta}}{\partial z}$	(10)

b. The physical implications of the model

The physical meaning of the turbulent mechanisms taken into account in this model appears clearly when examining mechanical energy budgets, i.e., mean kinetic energy (MKE), turbulent kinetic energy (TKE) and potential energy (PE) budgets. Diagnostic equations are given in Table 1 (cf. Mellor and Durbin, 1975).

Examination of Table 1 reveals two different categories of mechanisms: *local accumulations and spatial transfers* from one point to another of a given form of energy and *transformations* from a given form of energy into another one. Thus we can see transformation of MKE $[\overline{u'w'}(\partial\bar{U}/\partial z)+\overline{v'w'}(\partial\bar{V}/\partial z)]$ and PE $(-g\beta\overline{\theta'w'})$ into TKE, which according to (9) is immediately and locally dissipated into IE($\bar{\epsilon}$). These equations [(8)–(10)] evoke the following comments about the physical implications in the model under consideration:

1) Neglect of tendency and diffusion terms in the TKE equation means in particular that TKE flux produced by breaking surface waves and penetrative convection effects due to pronounced surface cooling cannot be taken into account.

2) The only source of TKE is local shear production $[\overline{u'w'}(\partial\bar{U}/\partial z)+\overline{v'w'}(\partial\bar{V}/\partial z)]$ plus buoyancy production or destruction $(g\beta\overline{\theta'w'})$.

3) The TKE equation thus expresses an instantaneous and local energy exchange between MKE, PE and IE (Fig. 1).

Thus the only role of turbulence in this model is to fix the *spatial transfer* of mean energies and the *local energy exchange* from MKE, into PE and IE; the level of these transfers and exchanges depend directly on local current shear and stability [Eqs. (3) and (4)]. More precisely, during the evolution of the marine upper layers subject to atmospheric forcings, turbulence acts as follows:

- In the mixed layer where (by definition) temperature gradients and the gradient Richardson number are very small, shear production and dissipation are of the same order of magnitude and more than an order of magnitude greater than buoyancy production (e.g., Mellor and Durbin, 1975). Therefore, the TKE equation expresses a direct local dissipation of MKE into IE. Then, with regards to temperature and current, turbulence driven by current shear act only to fix the spatial transfers of mean energies, which leads to *homogenization of the mixed layer.*
- In the thermocline, the current shear is important, leading to erosion and *entrainment* of the stable zone inside the mixed layer. This corresponds to a significant transfer of energy from MKE into PE,

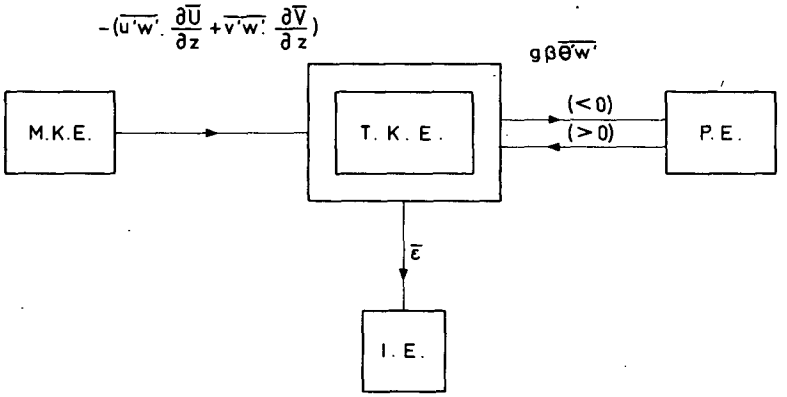

FIG. 1. Schematic representation of the turbulent kinetic energy budget in the model.

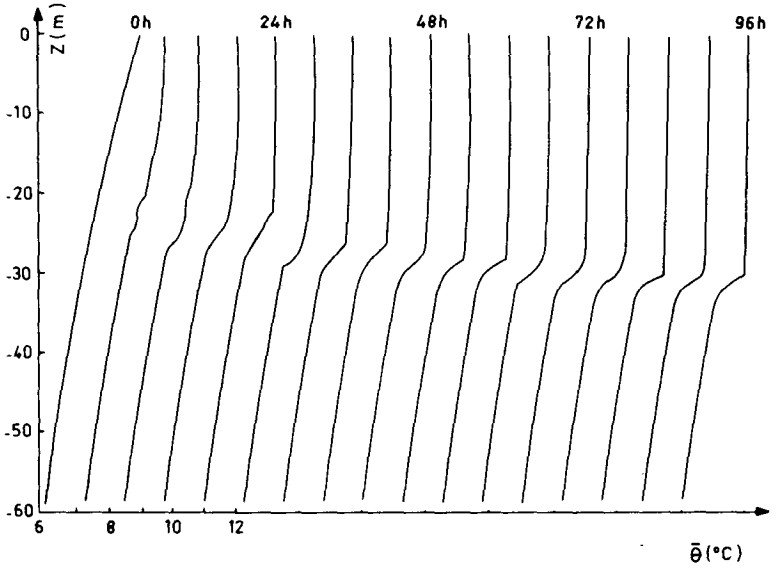

FIG. 2. Variation of temperature profile due to an impulsive wind and a zero surface heat flux. Profiles are plotted every 6 h, each one being displaced from the preceding one by 1.25°C.

through TKE. At the same time, turbulence intensity and diffusivity are decreasing until, at some depth, the critical Richardson number is reached; then local mixing is stopped.

It is interesting now to comment on the similitudes and differences between the present and "integral" models:

- The integral models assume that mean temperature and horizontal velocity are uniform within the mixed layer. This means that the spatial transfer of mean energies is immediately realized: this is not assumed in the present model where properties are locally calculated.
- Only the evolution of the mixed-layer bulk properties are calculated in integral models, and the results show a physically unrealistic discontinuity at the base of that layer. On the contrary, the present model predicts the progressive spatial decrease of turbulence below the mixed-layer base and therefore gives a better representation of the shape of the thermocline.
- The deepening of the mixed layer due to shear turbulence, to turbulent energy diffusion downward from the surface, and to penetrative convection, can be suitably parameterized in some integral models. The present one considers only shear and buoyancy turbulence productions and, from this point of view, looks like Pollard *et al.*'s (1973) model.
- It should be stressed again that because of the main assumption made in this approach, i.e., the universal character of the turbulence model adopted, no internal constants need to be adjusted. Note that this assumption is essential when such models are applied to geophysical situations in which no experimental data are available for a new adjustment. This is justified from the fact that the values proposed for these internal constants after quite different laboratory and atmospheric data present a weak dispersion (Rodi, 1979). Consequently, the critical value for the local Richardson number which is determined from the internal constants (Mellor and Yamada, 1974) does not need to be adjusted.

c. *Numerical solution*

The numerical solution of the two nonlinear parabolic-type partial differential equations, obtained when representing turbulence fluxes in Eqs. (1) and (2) by the above relationships, requires that they be in discrete form. An implicit scheme was selected for time differentiation, since this type of scheme does not *a priori* impose any stability constraint on the time step. Nevertheless, the presence in the dynamical equation of the term responsible for inertial oscillations leads to the selection of a so-called "implicit trapezoidal" method, and to consider numerical time steps lower than 3 h (Kurihara, 1965). The spatial differentiations were carried out with a finite-element method which makes it possible to introduce in a proper way surface conditions which are of a nonlinear Neumann type. The nonlinear nature of the equations, due to the diffusion operators in particular, necessitated the use of an iterative method for the estimation of turbulent fluxes.

The values of the physical constants in the equations are

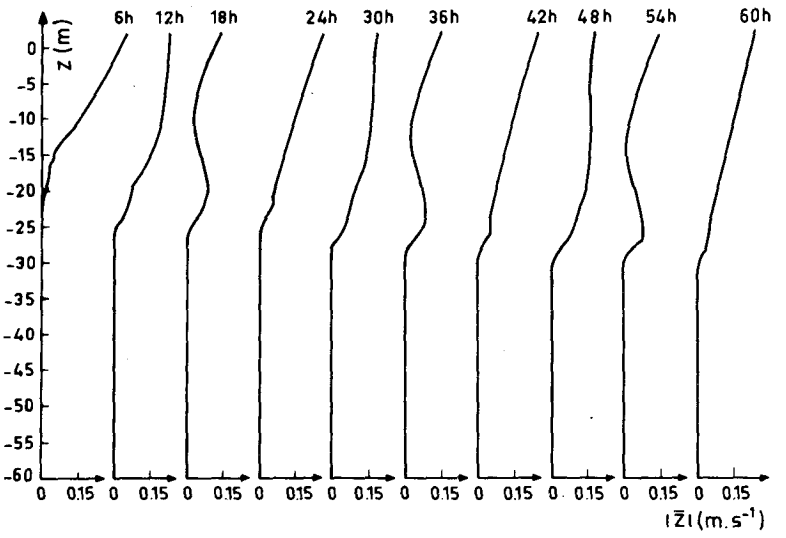

FIG. 3. Variation of current modulus profile due to an impulsive wind and a zero surface heat flux.

$$\left.\begin{aligned} &f = 10^{-4}\ \mathrm{s}^{-1}, \quad \beta = 1.73 \times 10^{-4}\ ^{\circ}\mathrm{C}^{-1} \\ &g = 9.81\ \mathrm{m\ s}^{-2}, \quad \nu = 0.134 \times 10^{-5}\ \mathrm{m^2\ s}^{-1} \\ &\chi = 0.134 \times 10^{-6}\ \mathrm{m^2\ s}^{-1} \end{aligned}\right\}$$

In most of the simulations discussed in Section 3, we set $D = 60$ m, as the thermocline only reaches that depth in certain special circumstances (in such cases, $D = 120$ m). Vertical grid resolution is set at 1 m. The duration of the simulations is set at 96 h, and the time step at 1 h. A computation time of some 48 s is required for a 96 h simulation using an IBM 370-168 computer with virtual storage.

3. The effect of air-sea transfer variability on the evolution of marine thermal structure

Several typical situations were simulated with the present model, first, in order to analyze the effect of wind-stress variability and, second, the effect of heat flux variability on the physical mechanisms governing the dynamic and thermal marine structure.

a. Effect of wind variability

Pollard and Millard (1970) and Gonella (1971) have already demonstrated the effect of the variability of local wind on the dynamics of marine upper layers. Pollard and Millard showed in particular that surface winds are responsible for the variability of inertial oscillations, and that the latter are mainly of local origin. Gonella states that the duration of local wind compared to the inertial period is a very important factor in the amplitude of inertial motions. The effect of wind variability on thermal structure, however, was not studied by these authors because of the nature of the models they used.

1) RESPONSE OF THE MARINE UPPER LAYERS TO AN IMPULSIVE WIND STRESS

The water mass is initially at rest with a stable temperature distribution (see Fig. 2). A constant surface stress τ corresponding to an 11 m s^{-1} west wind is applied after $t = 0$. The surface heat flux H is assumed to be zero at all times. The surface conditions can thus be written as

$$\left.\begin{aligned} \tau_x(t) &= \begin{cases} 0, & t \leq 0 \\ 2 \times 10^{-4}\ \mathrm{m^2\ s}^{-2}, & t > 0 \end{cases} \\ \tau_y(t) &= 0 \\ H(t) &= 0 \end{aligned}\right\} \quad (11)$$

It is to be noted that value attributed to $\tau_x(t)$, in fact, represents the square of the water friction velocity obtained using a drag coefficient $C_{10} = 1.3 \times 10^{-3}$.

Fig. 2 shows that the mixed layer thickens very rapidly during the first few hours and more slowly later. Examination of Figs. 3 and 4 reveals what happens more precisely. Initially, the surface layers are set in motion by the wind stress; the turbulence level is important due to a strong current shear (Fig. 3) and a small positive Richardson number (initial hydrostatic stability being not very important), giving rise to a rapid erosion of the stable layers. After several hours, we can see a mixed layer more than 20 m deep which is capped below by a well-marked thermocline (Fig. 2). At this level, the current shear is then associated with a strong temperature gradient, leading to an important energy exchange be-

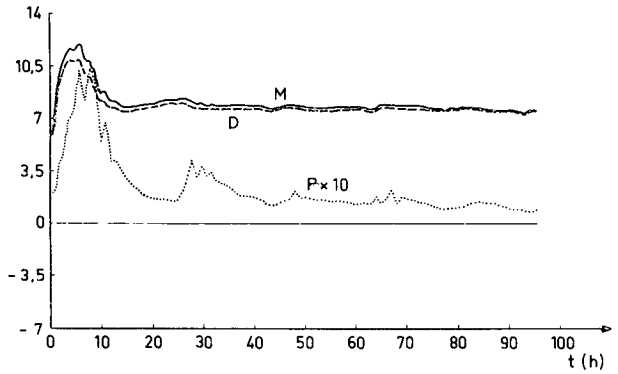

FIG. 4. Vertically integrated terms of kinetic energy budget:

$$P = \int_{-\infty}^{0} g\beta\overline{\theta' w'}\,dz,$$

$$M = -\int_{-\infty}^{0} \left(\overline{u'w'}\frac{\partial \bar{U}}{\partial z} + \overline{v'w'}\frac{\partial \bar{V}}{\partial z}\right)dz,$$

$$D = \int_{-\infty}^{0} \bar{\epsilon}\,dz.$$

Terms are nondimensionalized by U_*^3.

tween MKE and PE (Fig. 4), and therefore a much slower deepening of the mixed layer. Moreover, earth's rotation effects become significant on the current modulus profile (Fig. 3). Its nonuniform distribution is indeed constantly varying with a quasi-periodicity at the inertial period. At some times, we can see a minimum in the middle of the mixed layer and a more or less marked current shear at its bottom. This can be easily explained: the surface current generated by a constant wind action is turning in a clockwise direction within the Coriolis period. Thus, at certain times the wind stress is against the surface current and contributes to the deceleration of water mass movement and hence a diminution of the stored MKE. At other times the surface current is in the same direction as the wind stress, hence an increase of the stored MKE. This explains in particular the periodicity of the stored MKE, which is apparent in Fig. 3. Conversely, as can be seen in Fig. 4, integrated shear production is quasi-constant, whereas integrated buoyancy production (which in this simulation without surface heat flux represents mixed-layer deepening) is quasi-periodic.

When the wind stops after a given duration, the results indicate no further significant deepening of the mixed layer (Fig. 5). Turbulence dies out within a few hours and the water masses move following a residual current whose amplitude is directly related to the current modulus magnitude when the wind stops. If the wind stress duration is near an integer multiple of the inertial period, the final current amplitude will be relatively small (Fig. 6). If this duration is close to an integer plus one-half multiple of the inertial period, the final current amplitude will be high (Fig. 7). These results agree with those found by Gonella (1971) with respect to the amplitude of inertial oscillations as a function of the wind-stress duration. Examination of the evolution of temperature and current profiles reveals that the temperature gradient decreases within the thermocline as well as the mean velocity gradient close to it. However, for the first case (Fig. 6) the residual nonuniform current distribution presents a maximum amplitude velocity near $z = -25$ m, whereas in the second case (Fig. 7) the velocity is nearly

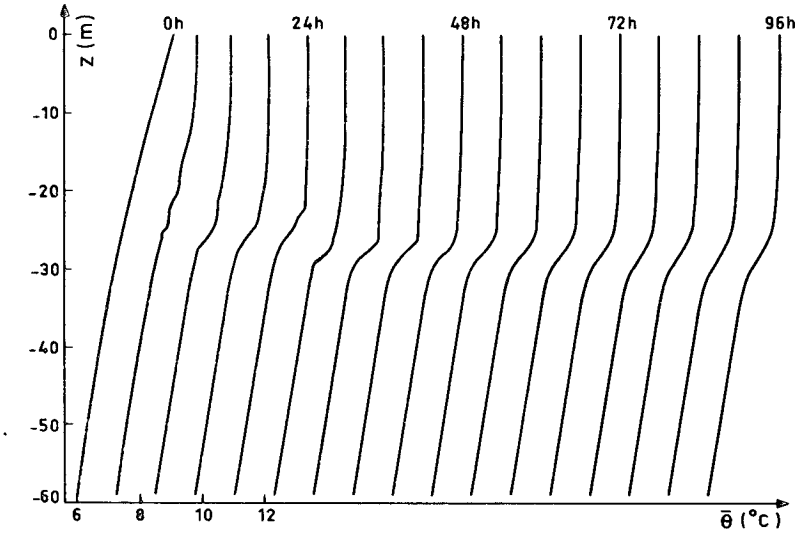

FIG. 5. Variation of temperature profile when the winds stops at $t = 35$ h. Profiles are plotted every 6 h, each one being displaced from the preceding one by 1.25°C.

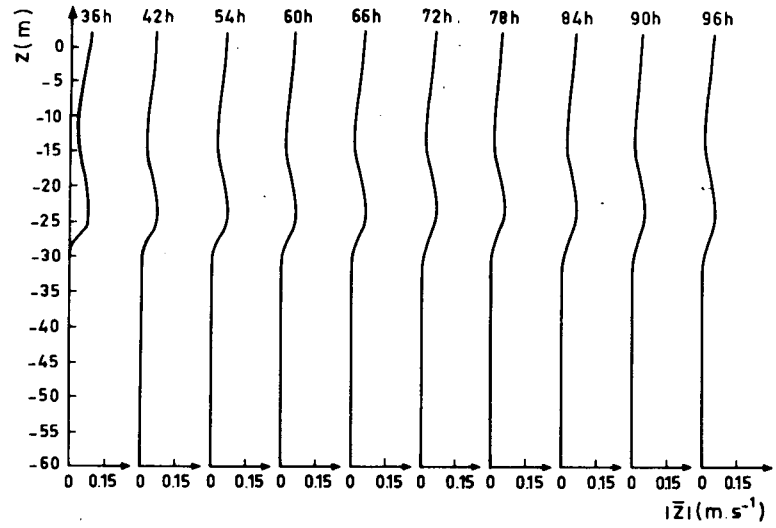

FIG. 6. Variation of current modulus profile when the wind stops at t = 35 h.

constant in the mixed layer which seems to move like a slab. This whole picture can be explained as follows: when the wind ceases so does the surface stress, causing some homogenization of the current field, a decrease of turbulence intensity, and a small spatial transfer of mean energies within the mixed layer. At the mixed-layer–thermocline interface, there exists at first some turbulent mixing due to the existing current shear, and because of an insufficient supply of MKE through the mixed layer there is a decay of the temperature and velocity gradients. At a later time, the residual current shear is too small with respect to stability, leading to a local Richardson number > 0.23. Thus turbulence dies out which explains the residual thermocline and the free inertial movement of water masses.

The diversity of these results shows that the marine thermal and dynamic structure is influenced not only by the nature and amplitude of atmospheric forcings, but also by the characteristic time scales of the marine environment, such as the inertial period. This leads us to examine the long-term effect of the wind-stress variability on the thermal and dynamic structure of marine upper layers.

2) THE INFLUENCE OF WIND ACTION PERIODICITY ON MIXED-LAYER DEEPENING

For a wind of given intensity and direction, appearing and disappearing at regular intervals, it is of interest to see if the characteristic period of the wind action has any long-term effect on the mixed-layer

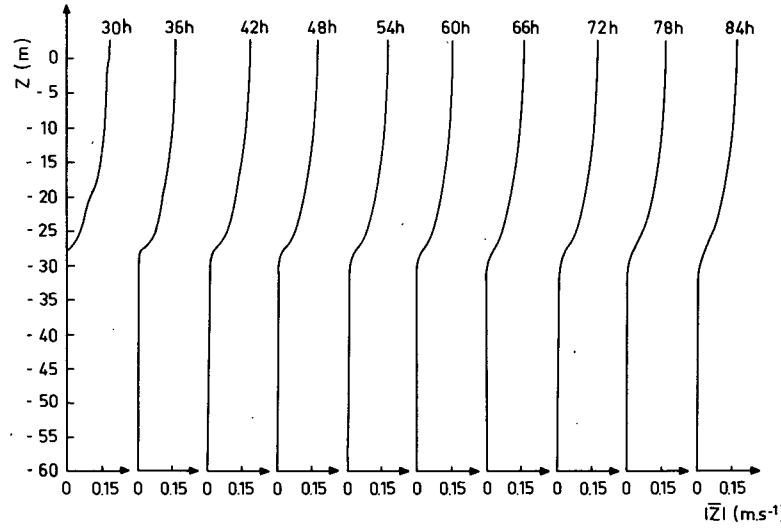

FIG. 7. As in Fig. 6 except at t = 30 h.

depth. Several simulations were carried out to this end, wherein the surface heat flux was kept at zero, and the action of the wind was assumed to obey the relationship

$$\tau_x(t) = \left\{ \begin{array}{l} 2 \times 10^{-4}\ \mathrm{m^2\ s^{-2}}, \\ \qquad nT < t \leqslant (n + \tfrac{1}{2})T \\ 0, \quad (n + \tfrac{1}{2})T < t \leqslant (n + 1)T \end{array} \right\}, \quad (12)$$

$$\tau_y(t) = 0$$

where n is an integer number and T the constant time period characterizing each simulation (Fig. 8). The values selected for T were 4, 8, 12, 14, 16, 18, 20, 22, 24 and 32 h. A simulation was also performed with $\tau_x(t) = 1 \times 10^{-4}\ \mathrm{m^2\ s^{-2}}$, which corresponds to $T = 0$. Each simulation lasted 96 h.

Fig. 8 shows the final depth attained by the mixed layer as a function of the wind sequence periodicity. The effect of this periodicity on the average thermal stratification evolution appears to be quite significant. For short periods ($T < 8$ h), the average mixed-layer deepening is of the order of 22 m. For wind sequences with the longest periods ($T > 24$ h), the final mixed-layer depth stabilizes at ~28–30 m. When the excitation frequency comes close to the inertial frequency, a resonance mechanism is observed, resulting in a much larger deepening of the mixed layer, attaining 78 m at $T = 18$ h.

The explanation is the following. As noted before, the horizontal current is turning in a clockwise direction within the inertial period. When the wind action period is equal to the inertial period, the surface current is always in the same direction as the effective wind stress, giving rise to a constant supply of MKE and a resulting strong current shear close to the thermocline. This can be seen in Fig. 9 which represents current modulus profile evolution for $T = 18$ h. The current distribution appears to be quasi-stationary.

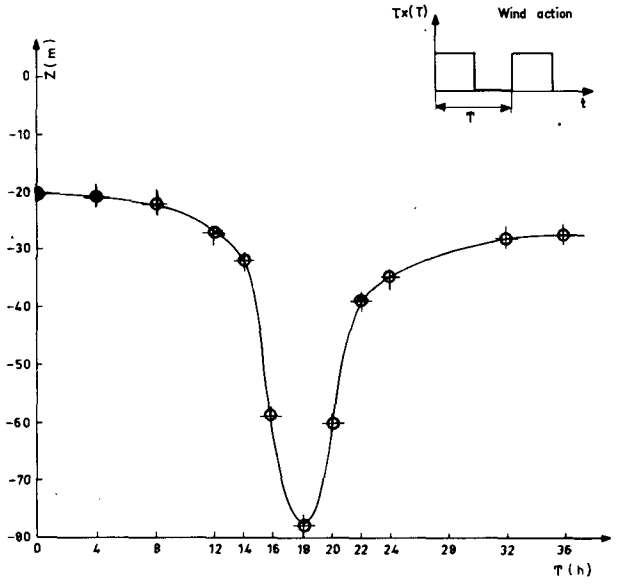

FIG. 8. Final characteristic depth of the mixed layer, after a 96 h simulation, in terms of the time period T of the wind sequence.

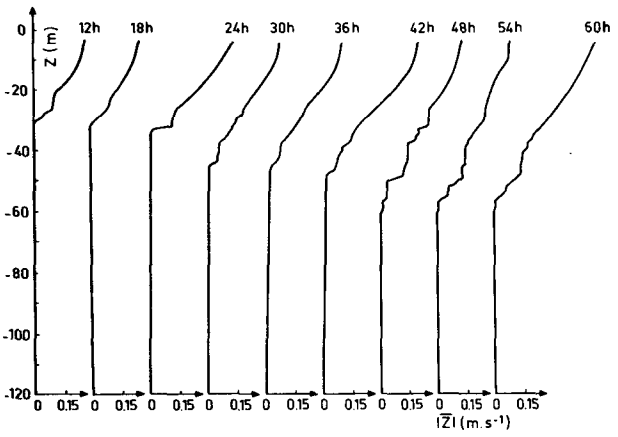

FIG. 9. Variation of current modulus profile when $T = 18$ h.

These results illustrate again the necessity of taking into account the interaction between the wind action variability and the marine characteristic time scales.

b. Effect of surface heat flux variability

We know (e.g., Mellor and Durbin, 1975) that the effect of a negative surface heat flux (heating) is to create a transient thermocline whereas a positive heat flux (cooling) leads to a deeper and colder mixed layer. However, it is worthwhile to investigate in detail the effect of surface heat flux on turbulent mixing and the global effects of surface heat flux variability. Therefore two simulations were carried out where the wind stress is constant and a non-radiative surface heat flux is either set to be zero or harmonic, with a 24 h period and a zero mean value:

$$H(t) = 0$$

or

$$H(t) = 6 \times 10^{-5} \sin\left[\frac{2\pi}{T}(t)\right] [\mathrm{^\circ C\ m\ s^{-1}}], \quad (13)$$

with $T = 24$ h. The wind speed is 3 m s^{-1}, corresponding to (with $C_{10} = 1.5 \times 10^{-3}$)

$$\tau_x(t) = 0.17 \times 10^{-4}\ \mathrm{m^2\ s^{-2}}, \quad \tau_y(t) = 0.$$

After 96 h of simulation, the depth and temperature of the mixed layer do not seem to be affected by the diurnal heat flux variability. This should not be too surprising since the overall heat balance remains zero in both simulations. A more detailed analysis, nevertheless, shows that the instantaneous

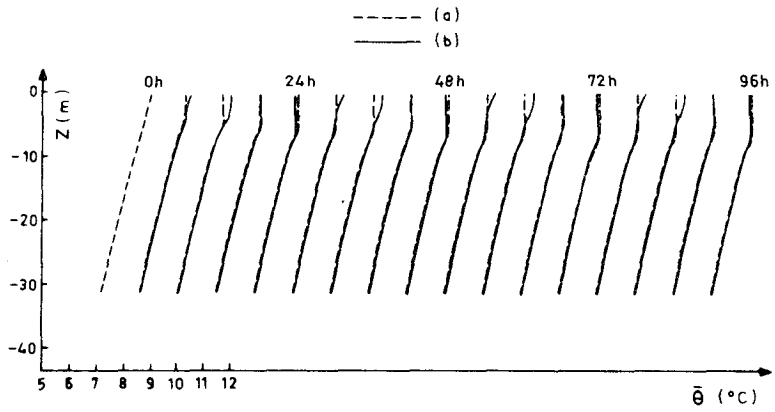

FIG. 10. Variation of temperature profile due to a light impulsive wind [$\tau_x(t) = 0.17 \times 10^{-4}$ m^2 s^{-2}, $\tau_y(t) = 0$] for (a) a zero surface heat flux, and (b) a sinusoidal surface heat flux (period is 24 h and amplitude is $H_0 = 6 \times 10^{-5}$ °C m s^{-1}).

thermal structure of the water mass can vary significantly from one simulation to the other. A certain diurnal variability of the sea surface temperature and of the instantaneous mixed-layer depth is evident in Fig. 10. When the surface heat flux is negative, there is a well-marked stratification in the first few meters and when the surface flux is positive there is complete mixing down to 6 m.

This can be explained as follows: under the effect of surface heating (daylight) turbulence intensity in the mixed layer is decreased due to a negative buoyancy production; shear production close to the surface is not sufficient to overcome the stability and turbulence locally dies out. Thus, the effect of heating is confined within the first meters leading to a transient thermocline formation. Conversely, under the effect of surface cooling (night situation), the buoyancy production is positive and thus increases the turbulence intensity within the mixed layer. Homogenization of the mixed layer is then observed and a more important current shear close to the thermocline leads to a more important mixed-layer deepening. So the main effect of the surface heat flux is to affect the turbulence intensity within the mixed layer and therefore the spatial transfer of mean energies. Nevertheless, simulation results with this model do not indicate any significant long-term effect of diurnal heat flux variability with respect to mixed-layer depth and averaged temperature distribution.

In addition it should be noted that the surface heat flux is generally determined from observed meteorological parameters, calculated sea surface temperature and the use of nonlinear computation formulas. As a consequence, the variability, on the scale of a few hours, of the meteorological parameters and the resulting surface heat flux will have a net effect on the global surface heat balance. Indeed, the latter has a significant impact both on the depth reached by the mixed layer and on the final temperature of that layer after a given period of time.

c. *Conclusions*

A rather simple model similar to the one by Mellor and Durbin (1975) is used to calculate the local evolution of temperature and drift current in marine upper layers subject to variable atmospheric forcings at the surface. Temperature and horizontal velocity fields, clearly non-uniform and constantly varying even with constant local atmospheric forcing, are dependent on the fundamental inertial period, and various simulations have revealed an appreciable long-term effect of the wind action variability on the scale of a few hours. This clearly demonstrates the interaction between air-sea transfer variability and marine dynamics; a good simulation thus needs a worthy representation of this interaction, particularly to take into account the phase difference between surface wind stress and current. This is very important as for the choice of the time resolution in the models. It is thus necessary *a priori* in any simulation to make use of meteorological observations with a periodicity which does not exceed a few hours.

4. Modeling the evolution of thermal stratification on the Gulf of Lion during the COFRASOV II expedition

a. *Description of observations collected from laboratory buoy BORHA II*

The data used were collected by the Laboratoire d'Océanographie Physique (LOP) du Muséum National d'Histoire Naturelle, Paris, in the northwest Mediterranean basin from the Laboratory Buoy BORHA II (42°N, 4°45'E) during July 1976. These observations include hourly measurements of the

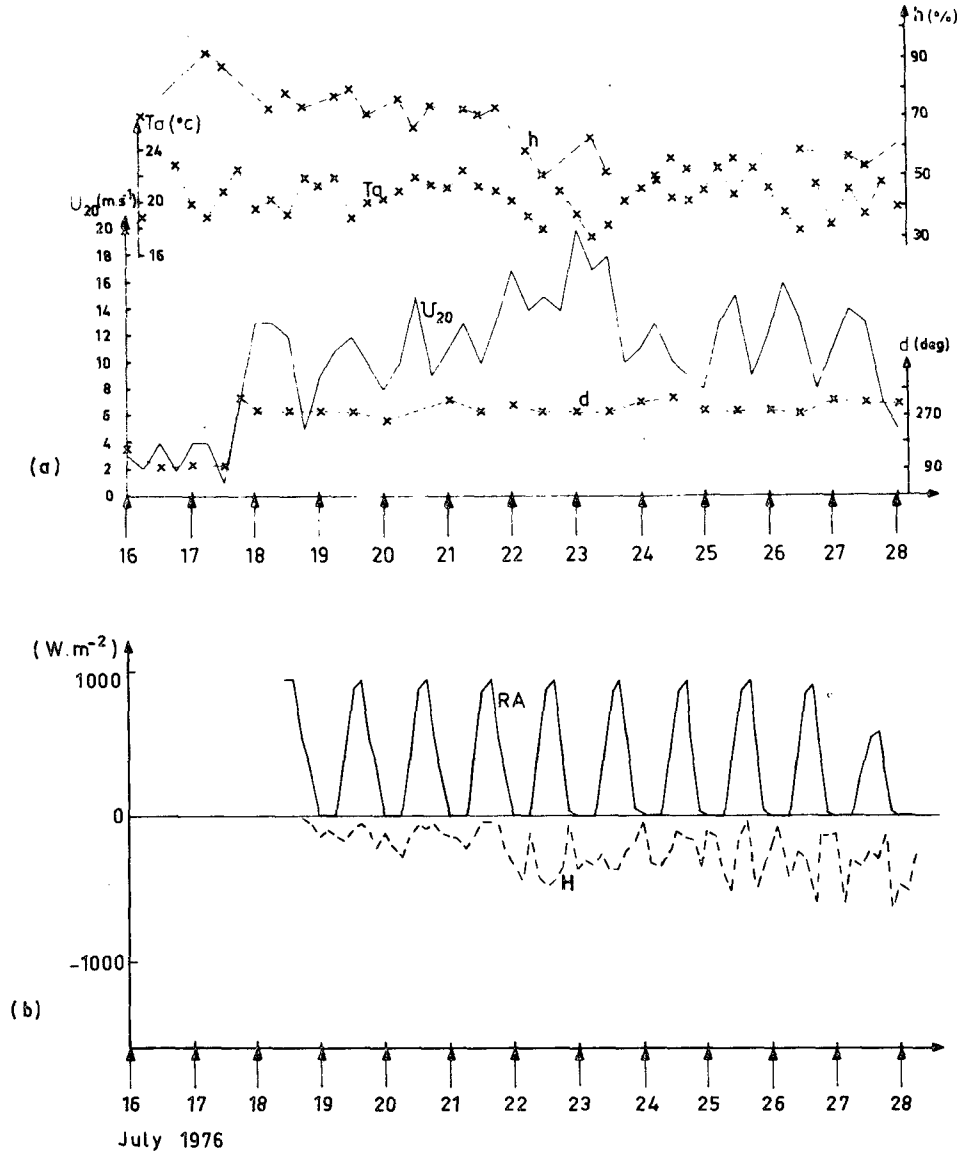

FIG. 11a. Temporal variation of wind speed and direction (U_{20} and d), dry-bulb temperature (T_a) and relative humidity (h) during COFRASOV II.

FIG. 11b. Evolution of the surface solar radiative flux (RA) and budget (H) of infrared radiative and turbulent latent and sensible heat fluxes computed from meteorological data and calculated sea surface temperature.

meteorological parameters in the atmospheric surface layer and measurements of sea temperature profiles performed every 2 h. The weather was very sunny and windy during this period, and was preceded by a period of light winds (see Fig. 11). The evolution of the marine thermal structure determined from bathythermographs reveals an 11 m deepening of the mixed layer within 10 days and a sea surface temperature drop of 2°C during that period. The time-depth isothermal contours beneath the thermocline do not on the average have a constant depth, which seems to indicate the presence of some advection phenomena (Fig. 12).

b. Numerical simulation runs

1) DETERMINATION OF INITIAL AND BOUNDARY CONDITIONS

An initial representative temperature profile is directly determined by smoothing the first available data over an 18 h period. An initial current profile is set up using the model by beginning the simulation

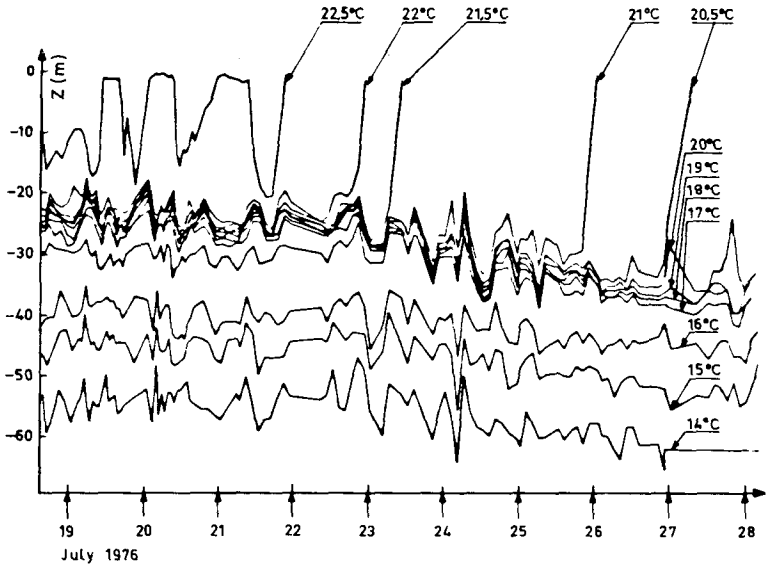

FIG. 12. Observed time-depth isothermal contours during COFRASOV II.

24 h earlier. The radiative and turbulent fluxes at the interface (Fig. 11b) are determined every hour from meteorological data measured in the atmospheric surface layer (wind, humidity, air temperature, cloud cover and atmospheric pressure), and from the computed sea surface temperature. A Bowen ratio is used when humidity data are missing. Incident solar radiation was estimated after Perrin De Brichambaut (1975), and its penetration into the water was parameterized by the expression given by Paulson and Simpson (1977) for very clear waters, i.e.,

$$R(z) = R(0)[0.4 \exp(0.2z) + 0.6 \exp(0.025z], \quad (14)$$

where $R(0)$ designates solar radiation incident on the water surface (considering the albedo), and $R(z)$ is the solar radiation penetrating to depth z. The balance of longwave radiation (atmospheric radiation plus sea surface radiation) was calculated after Swinbank (1963). The momentum and sensible and latent heat fluxes were calculated using classical bulk aerodynamic formulas. These formulas bring into play an exchange coefficient C_{10}, for which a value of 1.7×10^{-3} was selected. The depth chosen for the specification of "deep water" boundary conditions is here 60 m: water temperature at this depth is assumed to be constant and the same as deter-

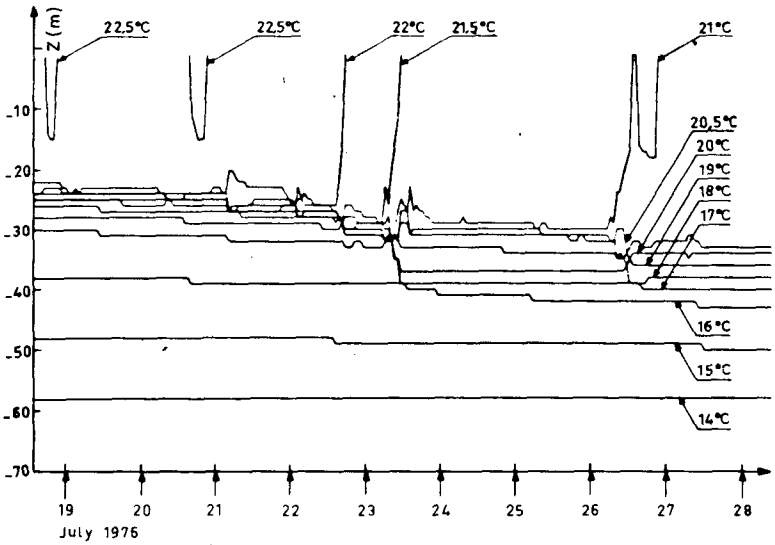

FIG. 13. Computed time-depth isothermal contours during COFRASOV II.

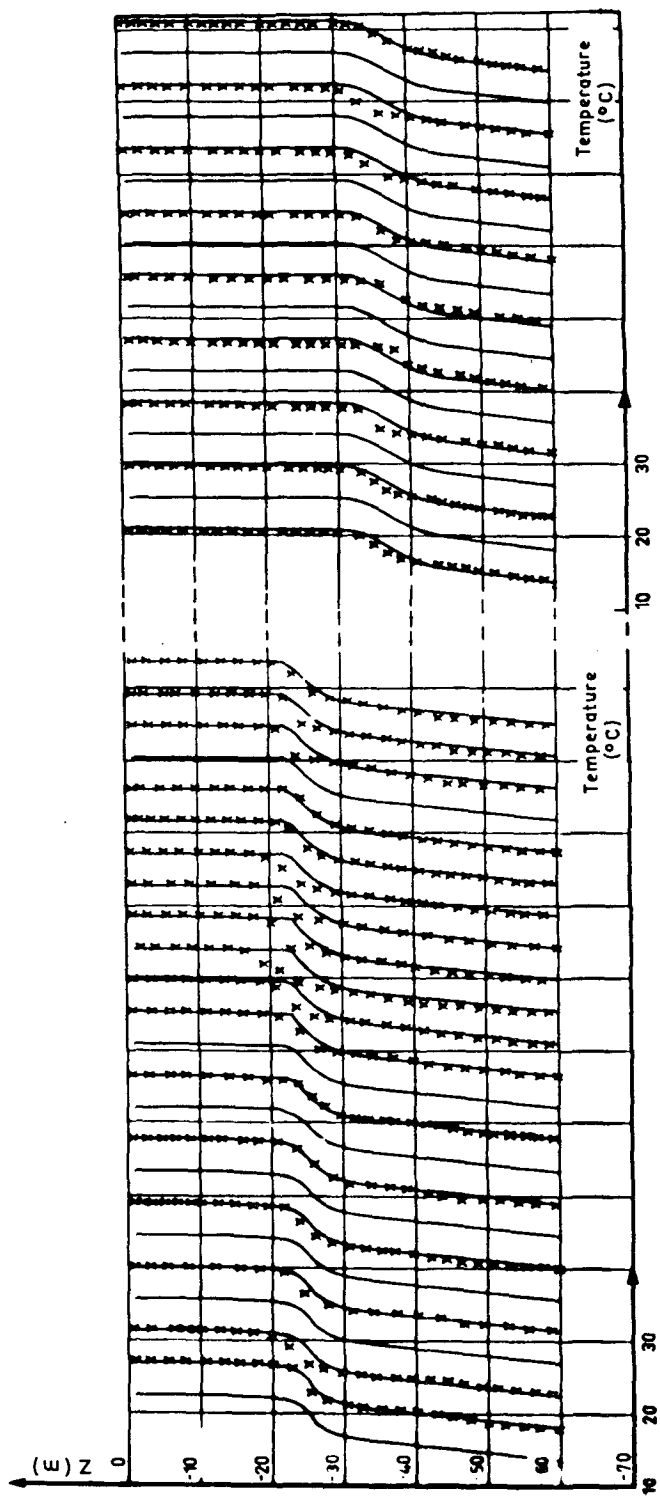

FIG. 14. Time variation of measured (×'s) and computed (solid line) temperature profiles at the beginning (a) and at the end (b) of the simulation. In each part, computed temperature profiles are plotted every hour. Each one is displaced from the preceding one by 4.4°C.

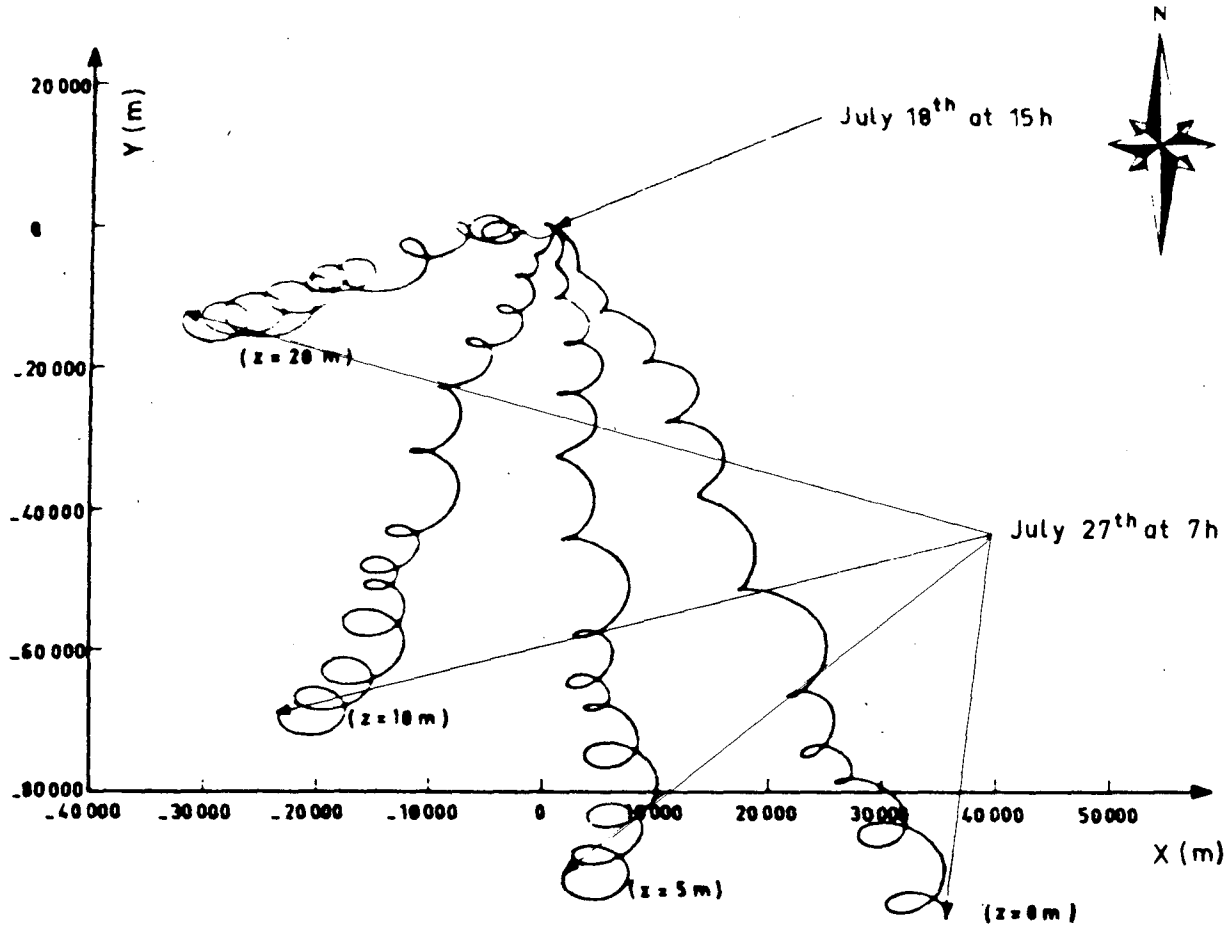

FIG. 15. Progressive vector diagram of currents computed at 0, 5, 10 and 20 m depth.

mined initially, i.e., 13.7°C. Drift current velocity at 60 m was considered to be zero.

2) RESULTS

The numerical simulation concerns the period from 1500 GMT 18 July 1976 to 0600 GMT 28 July 1976. The selected time step is 1 h, the grid spacing 1 m. Time-depth isothermal contours from calculated profiles (Fig. 13) are not modulated by internal waves, these being ignored by the model. Below the thermocline, they have on the average an almost constant depth, inasmuch as the advection phenomena are not taken into account by the model. It is to be noted that the temperature gradient within the thermocline is a great deal smaller after 23 July than the one shown by the measurements. As can be seen in Fig. 12, the evolution of the thermocline appears to follow the 18 and 19°C isotherms. A comparison between the mean changes in these two experimental curves and the evolution of the computed 18.5°C isotherm permits a judgement on the quality of the modeling.

Another criterion is a comparison between measured and calculated sea surface temperatures. As shown by Figs. 16a and 17a, there is a rather satisfactory overall agreement between observations and model results, both with respect to surface temperatures (even though there is a difference of some 0.3°C on the last day), and the deepening of the thermocline (in spite of a slight lead of the model with respect to reality). It can also be seen that the model reproduces well the distribution of temperature along the vertical (Fig. 14). Finally, the progressive current vector diagrams computed at various depths (Fig. 15) clearly demonstrate the inertial oscillations, and are quite similar to observations carried out at various occasions by the LOP in this area (Gonella, 1971). Unfortunately, no direct comparison can be made in the present case since current measurements are not available.

A more extensive comparison of results of the model to actual measurements is difficult because of the presence of advection phenomena. Nevertheless, the rather good estimates of the surface thermal evolution and the mixed-layer thickening

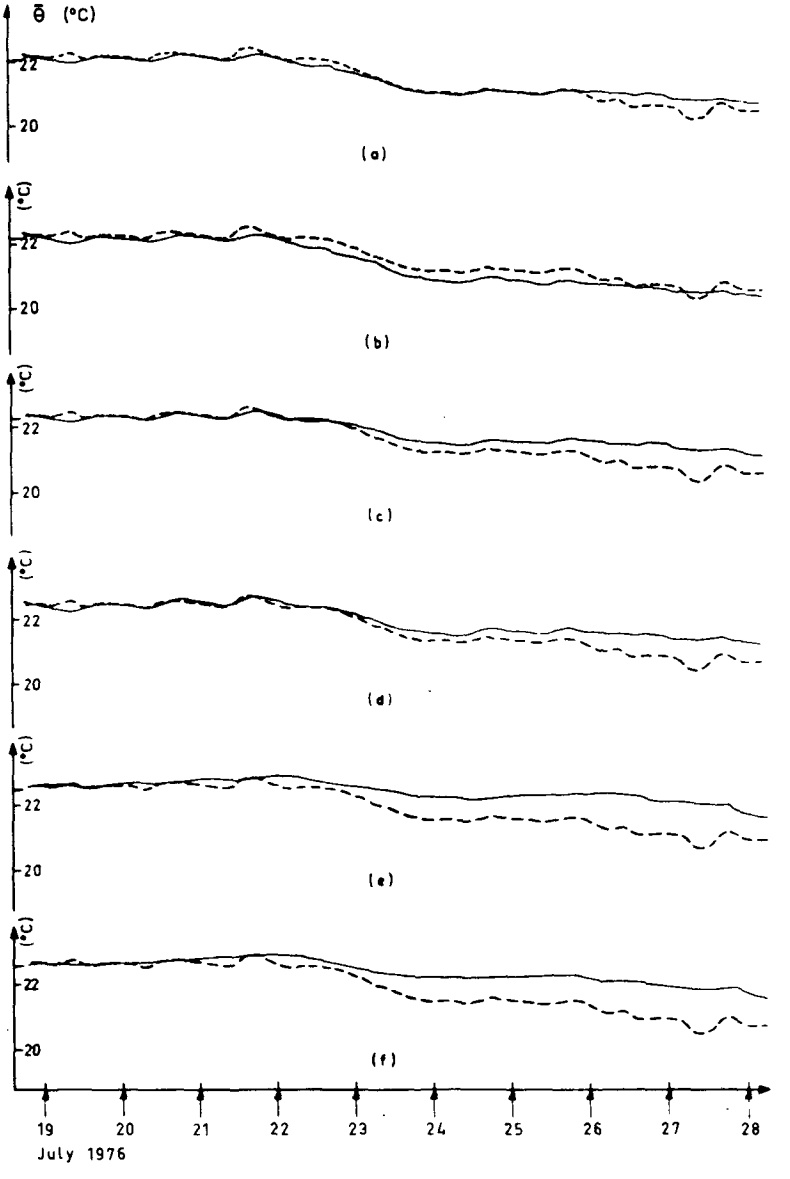

FIG. 16. Observed (dashed line) and computed (solid line) sea surface temperature:

(a) $C_{10} = 1.7 \times 10^{-3}$ and $R(z)$ = Eq. (14)
(b) $C_{10} = 2 \times 10^{-3}$ and $R(z)$ = Eq. (14)
(c) $C_{10} = 1.4 \times 10^{-3}$ and $R(z)$ = Eq. (14)
(d) $C_{10} = 1.7 \times 10^{-3}$ and $R(z)$ = Eq. (15)
(e) wind stress is averaged on a semidiurnal period
(f) wind stress is averaged on a diurnal period.

appear to indicate that local meteorological conditions actually had a dominant effect during the period under study.

c. *Analysis of the model's sensitivity to boundary conditions parameterization*

When simulating a real case, it seemed worthwhile to study the sensitivity of the model under use to boundary conditions. In particular, the effect of taking into account the time variability of air-sea exchanges was reexamined.

1) SENSITIVITY OF THE MODEL TO WIND-STRESS ESTIMATION

The value (1.7×10^{-3}) of the exchange coefficient employed in Section 4b, which is greater than the

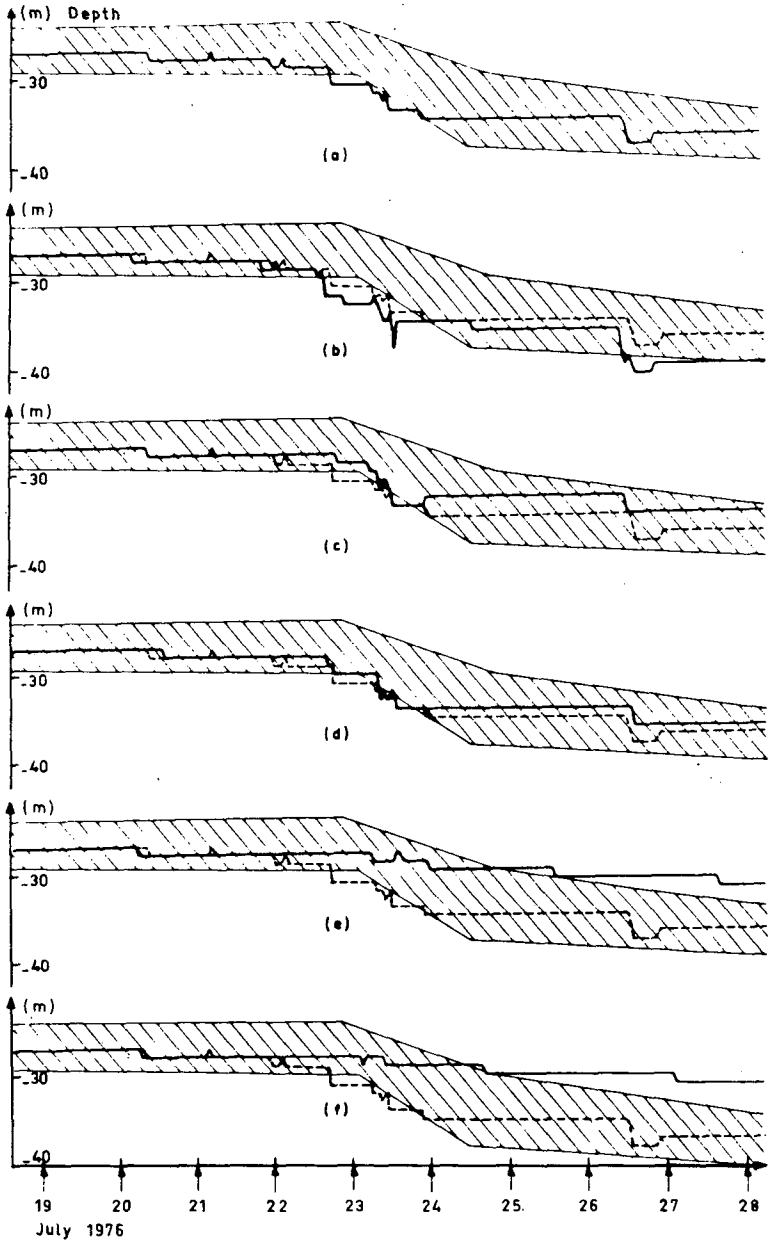

FIG. 17. Computed time-depth isothermal contour (18.5°C):

(a) $C_{10} = 1.7 \times 10^{-3}$ and $R(z)$ = Eq. (14)
(b) $C_{10} = 2 \times 10^{-3}$ and $R(z)$ = Eq. (14)
(c) $C_{10} = 1.4 \times 10^{-3}$ and $R(z)$ = Eq. (14)
(d) $C_{10} = 1.7 \times 10^{-3}$ and $R(z)$ = Eq. (15)
(e) wind stress is averaged on a semidiurnal period
(f) wind stress is averaged on a diurnal period.

The dashed line in Figs. 17b–17f is the computed time-depth isothermal contour 18.5°C of Fig. 17a. Hatched area shows the region where the small-scale variations of the measured time depth isothermal contours 18 and 19°C are located.

classical value (1.5×10^{-3}), was selected so that calculated results agree with observations. It is also to be noted that Mellor and Durbin (1975) have also used in their simulation a rather high exchange coefficient ($C_{10} = 2 \times 10^{-3}$). New numerical experiments have been performed with different exchange coefficients: $C_{10} = 1.4 \times 10^{-3}$ and $C_{10} = 2 \times 10^{-3}$. The results indicate that the model is quite sensitive

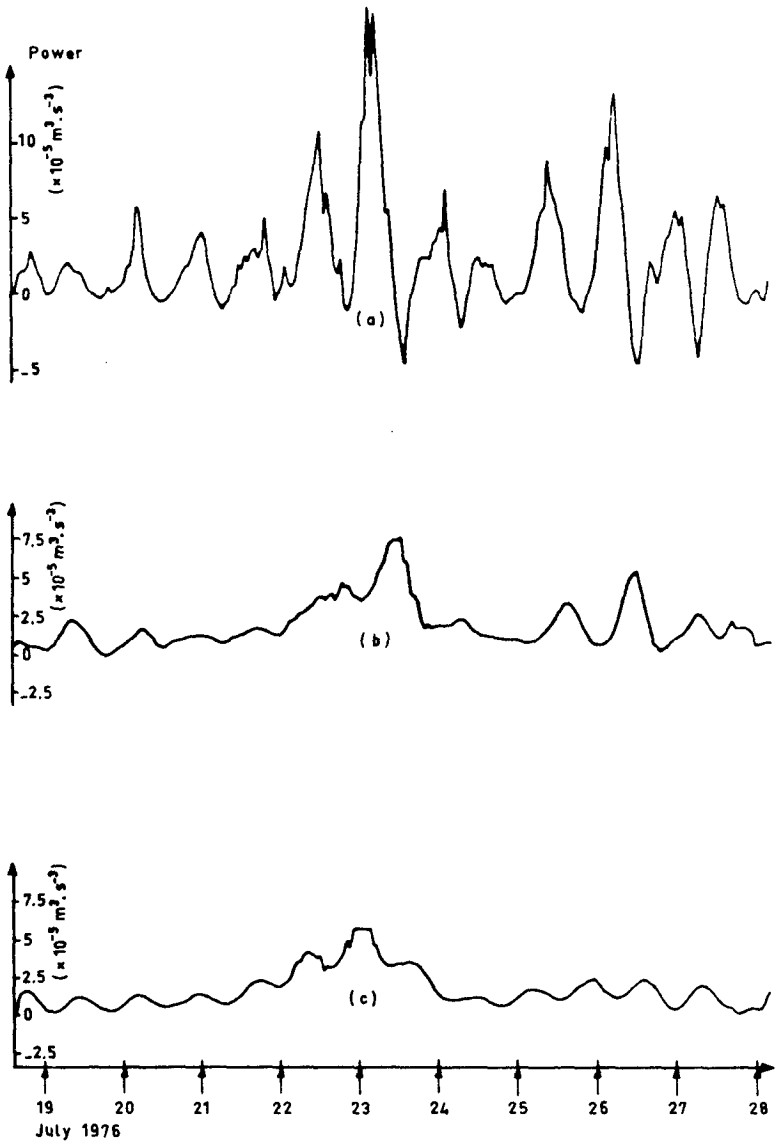

FIG. 18. Power supplied by the wind to the sea when (a) the wind stress is not averaged, (b) the wind stress is averaged on a semidiurnal period and (c) the wind stress is averaged on a diurnal period.

to the value adopted. The average final difference between calculated and measured sea surface temperatures changes sign when C_{10} goes from 2×10^{-3} to 1.4×10^{-3} (Fig. 16b and 16c); the final deepening of the thermocline also shows relative variations of 2–3 m in comparison to that calculated with a C_{10} of 1.7×10^{-3} (Figs. 17b and 17c).

These simulations thus demonstrate a rather strong (above the experimental uncertainty) sensitivity of the model to the parameterization of surface fluxes through the choice of the exchange coefficient. Increasing the latter has consequences similar to that of increased turbulent diffusivities in the model.

2) SENSITIVITY OF THE MODEL TO THE ESTIMATION OF SOLAR RADIATION PENETRATION

The coefficients selected for the calculation of solar radiation penetration were chosen because of the very clear water around BORHA II. A test, nevertheless, was carried out with an equation valid for more turbid waters [type IA in Jerlov (1968)'s classification]:

$$R(z) = R(0)[0.6 \exp(0.6z) + 0.4 \exp(0.05z)]. \quad (15)$$

Sea surface temperature (Fig. 16d) becomes slightly higher after 23 July 1976. The thermocline erosion is less pronounced, the difference attaining 1.5 m

(Fig. 17d). This is naturally due to the fact that the upper layers are more stable in more turbid waters. Thus, it appears that a precise parameterization of solar radiation penetration is required for a simulation of marine thermal structure. This means, for longer time simulation, that it is essential to include temporal turbidity variations, which can arise from primary production development.

d. Effect of air-sea transfer variability

Radiative and turbulent transfers at the air-sea interface were calculated every hour from meteorological parameters measured in the atmospheric surface layer and from the computed sea surface temperature. This 1 h time scale makes it possible to take into account not only the diurnal evolution of solar radiation but also wind variability throughout the day. In order to determine the effect of taking into account this short-term variability in weather conditions, two numerical experiments were performed in which meteorological parameters were averaged over periods of 12 and 24 h, respectively. In each case, the power supplied by the wind on the water surface was calculated from

$$E(t) = \left|\tau(t)\bar{Z}(0,t)\right|. \qquad (16)$$

The results of these simulations (shown in Figs. 16–18) indicate that when the meteorological parameters are averaged, the computed sea surface temperature is always above the measured surface temperature after 22 July 1976; the difference can reach 1.5°C (Figs. 16e and 16f). The thickening of the mixed layer is a great deal less when the averaging operator is applied; on 28 July the thermocline reaches a depth of 32 m for a 24 h average, instead of 37 m when no average is taken (Figs. 17e and 17f). The main effect of the averaging operator is to filter out the short periods during which the wind has a high velocity; the currents brought about within the mixed layer then have much lower amplitude and the power supplied by the wind $[E(t)]$ greatly diminishes (Figs. 18a, 18b and 18c). Furthermore, a comparison of the time evolutions of this power and the depth of the 18.5°C isotherm, in the case in which no averaging was performed, leads to the conclusion that the phases of thermocline deepening (in particular those of 1800 GMT 22 July, 0600 GMT 23 July and 1400 GMT 26 July) are well correlated with the power supplied by the wind, considering a 4 h lag (Figs. 17a and 18a).

One additional simulation was carried out while averaging only the heat fluxes in order to evaluate the effect of heat variability in comparison with mechanical energy transfer variability. A slight difference is noted with respect to the evolution of surface temperature. Otherwise, the results differ little, especially those concerning thermocline deepening.

Heat transfer variability thus appears to be of relatively little importance vis-à-vis momentum transfer variability. On the other hand, wind variability in this high wind situation looks very important. This indicates that strong winds during short periods have a determinant effect. Furthermore, it is important to describe correctly the interaction between wind and surface current.

5. Conclusions

We use in this work a model similar to that of Mellor and Durbin's (1975) in which local turbulent diffusivities are parameterized from current shear and stability functions obtained from second-order turbulence equations. This model also looks like that of Pollard *et al.* (1973) with respect to entrainment processes. Some improvements are made, in particular concerning the computational methods and the determination and inclusion of turbulent and radiative transfers at the air-sea interface. This model is used to calculate the local evolution of temperature and horizontal velocity of the marine upper layers subject to different atmospheric forcings.

Results of typical simulations with constant atmospheric actions reveal some diversity of temperature and current field evolution and in particular of current modulus variations within the mixed layer. Simulations with variable atmospheric forcings lead to the conclusion that the thermal and dynamic structure of the marine upper layers are affected not only by wind force but also by the periodicity of wind sequences. With regard to the long-term effect of heat flux variability, it is the overall level which appears to be the essential factor. The model is also used to reproduce the evolution of the thermal structure observed in the Gulf of Lion during the COFRASOV II expedition. Even though this approach is not able to reproduce all the realities of marine dynamics, the results are relatively satisfactory and seem to justify the selection of a one-dimensional time-dependent model. The sensitivity of the results to the penetration of solar radiation and to the parameterization of surface turbulent fluxes points out the necessity for accurate estimates of air-sea transfers. Here again, it appears essential to take properly into account the temporal variability of weather conditions.

The modeling of turbulent mechanisms, such as it is done here, is quite simplified. It has already been noted that the fact of ignoring the diffusion and tendency terms in second-order turbulence equations constitutes an excessive simplification and is probably responsible for the necessity to adopt a rather high exchange coefficient. It is clear that the effect of waves on the production and diffusion of turbulence from the surface, as well as countergradient transport and penetrative convection phe-

nomena, the seat of which is near to the thermocline, can only be suitably described within the context of genuine second-order turbulence modeling (cf., e.g., Siess, 1975; Zeman and Lumley, 1976). An improved model, explicitly taking into account diffusion effects for the variances of turbulent fluctuations, is being set up at present (Klein and Coantic, 1979).

Acknowledgments. This work has benefitted from the scientific guidance of Dr. Michel Coantic, of the Institut de Mécanique Statistique de la Turbulence, to whom we express our sincere appreciation and thanks. This study was in part carried out under E.D.F./I.M.S.T. Contracts 16336, 16175 and 16079. We extend our gratitude to Mr. Joseph Jacquet, Head of the Environnement Aquatique et Atmosphérique Department at Electricite De France. We also warmly thank the researchers of the Laboratoire d'Océanographie Physique of the Muséum National d'Histoire Naturelle for their advice and for providing us with the data from the COFRASOV II expedition.

REFERENCES

Andre, J. C., G. De Moor, P. Lacarrere and R. Du Vachat, 1976: Turbulence approximation for inhomogeneous flows. *J. Atmos. Sci.*, **33**, 476–491.

Camp, N. T., and R. L. Elsberry, 1978: Oceanic thermal response to strong atmospheric forcing. II. The role of one-dimensional processes. *J. Phys. Oceanogr.*, **8**, 215–224.

Coantic, M., 1978: An introduction to turbulence in geophysics and air-sea interactions. AGARDograph n°232.

Gonella, J., 1971: A local study of inertial oscillations in the upper layer of the ocean. *Deep-Sea Res.*, **18**, 775–788.

Jerlov, N. G., 1968: *Optical Oceanography*. Elsevier, 118–124 pp.

Klein, P., and M. Coantic, 1979: Modelling the mean and turbulent structure of the marine upper layers with a second-order turbulence closure. *Ocean Modelling*, No. 28, 7–10.

Kurihara, Y., 1965: On the use of implicit and iterative methods for the time integration of the wave equation. *Mon. Wea. Rev.*, **93**, 33–46.

Lumley, J. L., and B. Khajeh-Nouri, 1974: Computational modeling of turbulent transport. Turbulent diffusion and environmental pollution. *Advances in Geophysics*, Vol. 18a, Academic Press, 169–192.

Mellor, G. L., and P. A. Durbin, 1975: The structure and dynamics of the ocean surface mixed layer. *J. Phys. Oceanogr.*, **5**, 718–728.

——, and T. Yamada, 1974: A hierarchy of turbulence closure models for planetary boundary layers. *J. Atmos. Sci.*, **31**, 1791–1806.

Niiler, P. P., and E. B. Kraus, 1977: One-dimensional models. *Modelling and Prediction of the Upper Layers of the Ocean*, E. B. Kraus, Ed., Pergamon Press, 1977, 143–172.

Paulson, C. A., and J. J. Simpson, 1977: Irradiance measurements in the upper ocean. *J. Phys. Oceanogr.*, **7**, 952–956.

Perrin De Brichambaut, C., 1975: Estimation des ressources énergétiques solaires en France. Supplément aux Cahiers AFEDES, No. 1.

Pollard, R. T., and R. C. Millard, 1970: Comparison between observed and simulated wind generated inertial oscillations. *Deep-Sea Res.*, **17**, 813–821.

——, P. B. Rhines and R. O. R. Y. Thompson, 1973: The deepening of the wind-mixed layer. *Geophys. Fluid. Dyn.*, **3**, 381–404.

Rodi, W., 1979: Turbulence models for environmental problems. *Lecture Series 1979-2*, Von Karman Institute for Fluid Mechanics, Karlsruhe, Germany, 1–89.

Siess, J., 1975: Étude d'après la méthode de J. L. Lumley de la pénétration de la turbulence dans un milieu stratifié. Thèse Docteur-Ingénieur, Université Marseille.

Swinbank, W. C., 1963: Long-wave radiation from clear skies. *Quart. J. Roy. Meteor. Soc.*, **89**, 339–348.

Wyngaard, J. C., and O. R. Cote, 1974: The evolution of the convective planetary boundary layer. A higher-order closure model study. *Bound.-Layer Meteor.*, **7**, 289–308.

Yamada, T., and G. Mellor, 1975: A simulation of the Wangara atmospheric boundary layer data. *J. Atmos. Sci.*, **32**, 2309–2329.

Zeman, O., and J. L. Lumley, 1976: Modeling buoyancy-driven mixed layers. *J. Atmos. Sci.*, **33**, 1974–1988.

Zilitinkevich, S. S., D. V. Chalikov and Y. D., Resnyansky, 1979: Modelling the oceanic upper layer. *Oceanol. Acta*, **2**, 219–240.